ω-phase and solitary waves induced by shock compression of bcc crystals

Johannes Roth
Institut für Theoretische und Angewandte Physik, Universität Stuttgart, Pfaffenwaldring 57, 70550 Stuttgart, Germany
(Received 15 June 2004; revised manuscript received 31 May 2005; published 26 July 2005)

Molecular dynamics simulations show that shock waves in single crystals are frequently accompanied by solitary waves. Here we present results for bcc crystals where the atoms interact via the Dzugutov potential [M. Dzugutov, J. Non-Cryst. Solids **131**, 62 (1991)]. In general the shock waves cause a phase transformation to a close-packed phase. In addition, special phenomena occur if bcc is shocked along the threefold ⟨111⟩ direction. We observe an intermediate phase, which is identified as the so-called ω-phase, and closely related nonsteady solitary waves in the regime of overdriven shock waves. The phenomena are described in detail and compared to solitary waves in other materials. The origin and stability of the ω-phase are studied. We find that a single solitary wave mode exists parallel to the ⟨111⟩ direction, and solitary waves along other directions are derived from it. A simple collision model is presented that captures the essential properties of the solitary waves.

DOI: 10.1103/PhysRevB.72.014126 PACS number(s): 62.50.+p, 61.44.Br, 02.70.Ns

I. INTRODUCTION

In a related paper (called paper I in the following)[1] we have described phase transitions from bcc and other metastable phases to close-packed structures induced by shock waves. We mentioned the observation of nonsteady solitary waves along the threefold ⟨111⟩ direction, related to an intermediate phase into which bcc transforms at subsonic velocities. Since the solitary waves have been observed very frequently and for different structures and interactions, we decided to investigate this phenomenon in more detail.[2–4]

There may be objections to call the exceptional wave features solitary waves or even solitons since they do not fulfill the rigorous mathematical requirements. The solitary waves get damped, by virtue of the finite size of the samples and the discrete nature of the structure, temperature, and other influences. But this is the case in any physical system. The exceptional waves possess all the properties of solitary waves: they show up as separated maxima when they move through the undistorted or elastically compressed crystal, they show almost no dispersion, and their velocity depends on their height. Even the collision property could be demonstrated so that we may call them solitons and not only solitary waves.

With the advent of large massively parallel supercomputers it has become possible to carry out multimillion atom molecular dynamics simulations. One of the applications is to study the defects generated by shock waves on an atomistic scale in three dimensions. Before it was not possible to resolve the details of the defects,[5] and the simulations were limited to fourfold symmetry directions. Thus it occurred as a surprise when Germann *et al.*[2] found that simulations of one of the simplest systems, fcc crystals with Lennard-Jones interactions, already yielded quite complicated results if shocked along the ⟨111⟩ direction and ⟨110⟩ direction: elastic precursor waves, different slip systems, and martensiticlike phase transitions. The new phenomena are still only partially explained.[6–8] The surprise included nonsteady solitary wave trains along the twofold direction.[9] Further examples of solitary wave observations include simulations by Bringa *et al.*[10] in fcc copper, by Zybin *et al.*[4,11] in a diamond structure, and by Zhakhovskiĭ *et al.*[4,12–15] in fcc Lennard-Jones crystals. In all these cases an oscillatory behavior of the elastic wave preceeding the plastic wave was observed.

Solitons are well known from shock wave studies of one-dimensional models for a number of interactions.[16] They can be described as Korteweg–de Vries or Toda solitons depending on the nonlinearity and strength of the interaction.[17] The one-dimensional solitons are caused by the lack of plasticity. The same happens in the three-dimensional simulations mentioned above if the shock strength is below the Hugoniot elastic limit. The solitary wave train is now locked into a steady oscillatory profile.[9] Actually, solitary wave peaks are still visible in the elastic-plastic regime and in the overdriven regime as the results by Germann *et al.*,[2] Zybin,[4] and Zhakhovskiĭ *et al.*[12,13] show.

In addition to the locked-in solitary waves there are nonsteady waves[9,18,19] visible in the *elastic-plastic* regime. The nonsteady waves proceed ahead of the locked-in solitary waves. In Zybin *et al.*'s[4] and Zhakhovskiĭ *et al.*'s[12,13] simulations they are not visible since these authors are averaging observables like stress and temperature in a frame moving with the steady wave profile.

The results presented here are about nonsteady solitary waves in bcc along the ⟨111⟩ direction in the *overdriven* regime. Such solitary waves have also been observed in bcc iron along the ⟨111⟩ direction by Kadau[3,20] and by the present author in a simple cubic structure along the fourfold direction.

We can demonstrate that the nonsteady solitary waves are a supersonic continuation of a subsonic phase transformation that occurs in bcc only if shocked along the ⟨111⟩ direction. The origin of the phase transformation is an instability with respect to uniaxial compression of the bcc structure interacting by the Dzugutov potential. The instability is related to the softening of the longitudinal phonon mode. If this mode has the ideal wave vector $\frac{2}{3}[111]$, every second and third plane in bcc collapses. The result is the two-layer hexagonal ω-phase, the crystal structure of AlB_2 or ω-CrTi.[21] If the

wave vector of the phonon mode deviates from the ideal value, a modulated structure is observed. More precisely, a spatial sequence of bcc and the ω-phase occurs that leads to oscillatory pressure profiles. The formation of the ω-phase is not an artifact of the Dzugutov potential since it occurs frequently in bcc elements and bcc alloys upon cooling, quenching, or high pressure or shock compression.[22,23]

The difference between the formation of the modulated ω phase and the locked-in solitons is that the ω-phase spreads out at subsonic speed whereas the locked-in solitons move at the speed of sound.[2] The nonsteady solitary waves, on the other hand, are much faster than the plastic wave front, at least at high piston velocities in the overdriven range, and move far ahead of the plastic wave front through the undisturbed or uniaxially compressed material.

The paper is organized as follows. First we will describe the ω-phase observed in the underdriven regime together with the solitary waves in the overdriven regime. Next we will present the results for arbitrary directions and discuss the possibility of suppressing the solitary waves. Then we will study the origin and stability of the ω-phase and explain the solitary waves by a simple collision model. An analytical description will also be addressed. Finally we will discuss the different classes of solitary waves in one and three dimensions, and at the end we will compare the solitary waves to the results obtained by Kadau[3] for the same bcc structure but using embedded atom method (EAM) potentials fitted to iron.

II. GENERATION OF THE SHOCK WAVES AND SIMULATION SETUP

Details about the generation of shock waves, the interaction, and the simulation setup have been presented in paper I already. In the present work we have applied the momentum mirror method to generate the shock wave: the velocities of the atoms are inverted as soon as they reach the upper end of the sample. Thus the atoms behave as if a second sample is colliding with the simulated one. To study the stability and to answer the question whether the solitary waves may be a consequence of the infinitely large acceleration of the atoms at the beginning of the simulation, we invented a scheme where the samples do not collide at full speed at the beginning of the simulation but where the piston velocity (respectively the sample velocity) is increased linearly until the desired final velocity $u_{p,end}$ is reached. A variable is introduced, namely the time interval t_r of ramping up the velocity. To study the influence of the momentum mirror, the simulations have been supplemented by symmetric-impact runs.

For the simulation of shock waves it is necessary to apply periodic boundary conditions, otherwise the sample would expand laterally and eventually disintegrate. The direction of the shock wave is chosen parallel to one of the coordinate axes, for example the x axis. This limits the possible crystalline directions along which the shock wave can travel to the rational directions indexed by the Miller indices. In addition to the main symmetry directions studied in paper I we have carried out simulations along many other low-index directions to find out the dependency of the solitary wave amplitude on the orientation of the sample. The boundaries of the samples were open at the lower end of the sample and periodic along the two transverse directions.

The size of the samples depends on the orientation. Therefore we will not list all the numbers. Most of the simulations have been carried out with a small sample of about $20\times20\times100$ interatomic distances a containing of the order of 40 000 atoms. To study the influence of the sample size on the solitary waves, longer samples (of length $200a$, $300a$, and $600a$ with up to 250 000 atoms), thinner samples [with a cross section of $(6\times6)a^2$ and $(8\times8)a^2$] and thicker samples [$(40\times40\times300)a^3$ with 500 000 atoms up to $(120\times120\times600)a^3$ with 4.5 million atoms] have been used.

The Dzugutov potential applied for this study is similar to the Lennard-Jones potential down to its minimum at $r=1.061a$ (Ref. 39) and $V=-1\epsilon$. The minimum is followed by a maximum at $r=1.5282a$ and $V=0.7906$. The cutoff radius is $r_c=1.805a$. The ground state of the Dzugutov potential at low temperatures and pressures is the bcc structure. If the pressure is increased, a phase transformation is observed into a close-packed phase with a random stacking sequence.[1]

The simulations have been carried out at sample temperatures of $kT=0.001\epsilon$, established by equilibration before the shock wave simulations are started. If one assumes a binding energy of the order of 1 eV then the simulation temperature would correspond to 12 K. Simulations carried out at temperatures up to $kT=0.01\epsilon$ (120 K) do not change the behavior of the solitary waves, although damping is observed at higher temperatures, as discussed below.

III. GENERAL RESULTS FOR SHOCK WAVES ALONG THE ⟨111⟩ DIRECTION

The effect of shock waves on stable and metastable structures interacting via the Dzugutov potential have been described in detail for different crystal directions in paper I. A short summary of the results along the ⟨111⟩ direction will be given here. The Hugoniot diagram for shock waves in bcc along the ⟨111⟩ direction is represented in Fig. 1. There are three different regimes with respect to the piston velocity, but the lowest, elastic regime is not visible in the figure since it ends at $u_p/c=0.035$ already ($c=20.2v_0$ is the velocity of sound along the ⟨111⟩ direction). The underdriven regime with an elastic wave of velocity $u_s\approx c$ and a phase transition wave with increasing velocity follow up to a piston velocity of about $u_p/c\approx0.2$. Above $u_p/c\approx0.2$ we are in the overdriven regime. At the transition front the sample transforms first from bcc into a highly defective polycrystalline sample. An additional curve is plotted in Fig. 1 below the transition front: It marks the velocity with which the high-defect polycrystalline sample is transformed into a low-defect phase with few crystallites.

Further wave fronts are drawn in Fig. 1: The velocity with which the three-layer bcc phase is transformed into the ω-phase and the velocity of the fastest solitary wave train. Both curves meet at about $u_p/c=0.185$ where they cross the velocity of sound. This is a clear indication that both phenomena are related. Between $u_p/c\approx0.2$ and $u_p/c\approx0.3$ up to four additional solitary wave maxima, slower than the first

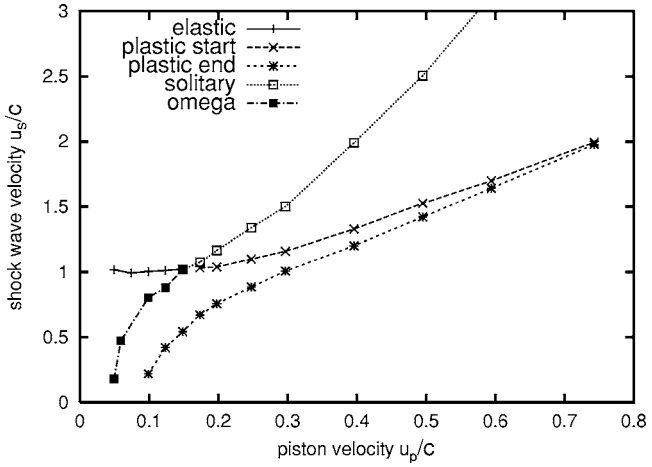

FIG. 1. Hugoniot diagram for shock waves along the ⟨111⟩ direction in the bcc crystal. The axes are scaled with the velocities of sound. The plus signs indicate the velocity of the elastic and transition wave fronts; the crosses indicate the speed with which the high-defect phase transforms into a low-defect structure. The stars and the squares indicate the propagation velocity of the fastest solitary wave and the spreading of the ω-phase, respectively.

solitary wave but faster than the transition front, can be distinguished. The velocities of the latter have not been included for clarity.

A. Evolution of the hydrostatic pressure profile with increasing piston velocity

The formation of the ω-phase and the evolution of the solitary waves can be described by means of the hydrostatic pressure as a function of increasing piston velocity. The representative cases are summarized in Fig. 2.

Case (1) $u_p/c=0.005-0.035$: Only a dispersive nonsteady elastic precursor wave exists. At about $u_p/c=0.035$ the hydrostatic pressure reaches the transition pressure from bcc to the close-packed phase. A phase transition to a close-packed phase would be expected now, but it is delayed by the creation of the intermediate ω-phase.

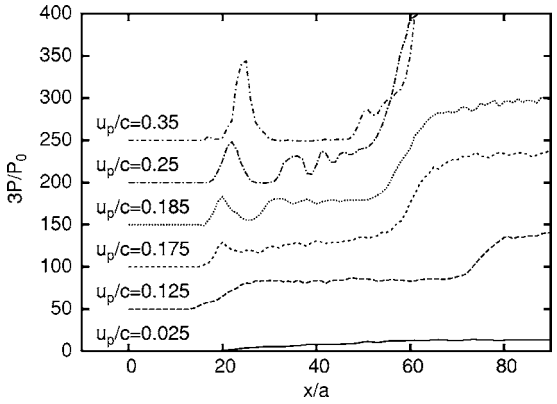

FIG. 2. Hydrostatic pressure profiles as a function of u_p/c at arbitrary simulation times. The shock wave is moving to the left. The curves have been shifted by $50P_0$ with respect to the following one to avoid overlaps.

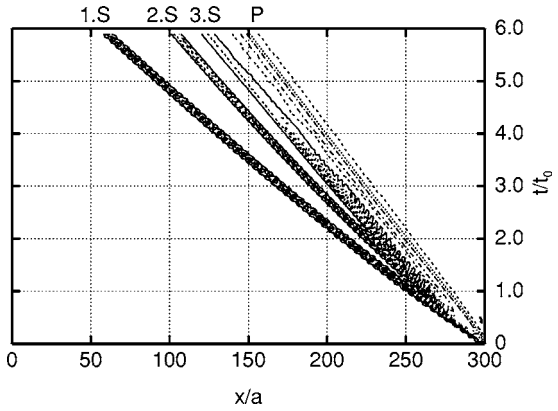

FIG. 3. Hydrostatic pressure as a function of time and path. Contours are plotted at $10/3\ P_0$. Temperature $kT=0.001\epsilon$, the piston velocity is $u_p/c=0.25$. Three solitary wave peaks (1.S, 2.S, and 3.S) are visible in front of the transition wave front (P).

Case (2) $u_p/c=0.035-0.175$: A plateau is observed between $x/a=20$ and 70, which is caused by the ω-phase. The new phase is most prominent around $u_p/c=0.1$ and is subsequently transformed into fcc by the transition wave. The pressure in fcc is lower than in the new phase if u_p/c is below 0.075 and higher otherwise. The ω-to-fcc transition is too slow in this range to be determined accurate enough. Thus it is not shown.

Case (3) $u_p/c=0.175$: A peak starts to grow at the front of the plateau, which is the precursor of the first solitary wave. At about $u_p/c=0.185$, the separation becomes apparent.

Case (4) $u_p/c=0.2-0.3$: The first solitary wave is well separated from the plateau that is no longer flat but modulated, indicating the nucleation of further solitary wave peaks at higher piston velocities. The distance between the solitary wave peaks and the phase transition front grows with simulation time.

Case (5) $u_p/c=0.3-0.75$: Only the first solitary wave remains stable, all the other solitary waves decay or are overtaken by the transition front.

Up to four oscillation maxima have been observed. Their width shrinks when they develop into solitary wave peaks. Within the maxima the ω-phase is found and the bcc phase is in between. Since the whole configuration is moving, this is a clear hint that the transition is reversible.

1. Velocities of the solitary waves

The velocity of the solitary wave peaks is related to their height: The higher a peak is, the faster it moves. Since the trailing peaks are lower than the first one they also move slower. The velocities and heights of a specific solitary wave peak are not constant but decrease very slowly with time. This can be seen if Fig. 3 is held at a glancing angle. The solitary waves that emerge from the transition front may be overtaken again by the transition front after some time. At low temperature the height of the first solitary wave is constant during simulation time and the width is about $4a$. The other solitary waves also have constant height, and their width is about $5-6a$.

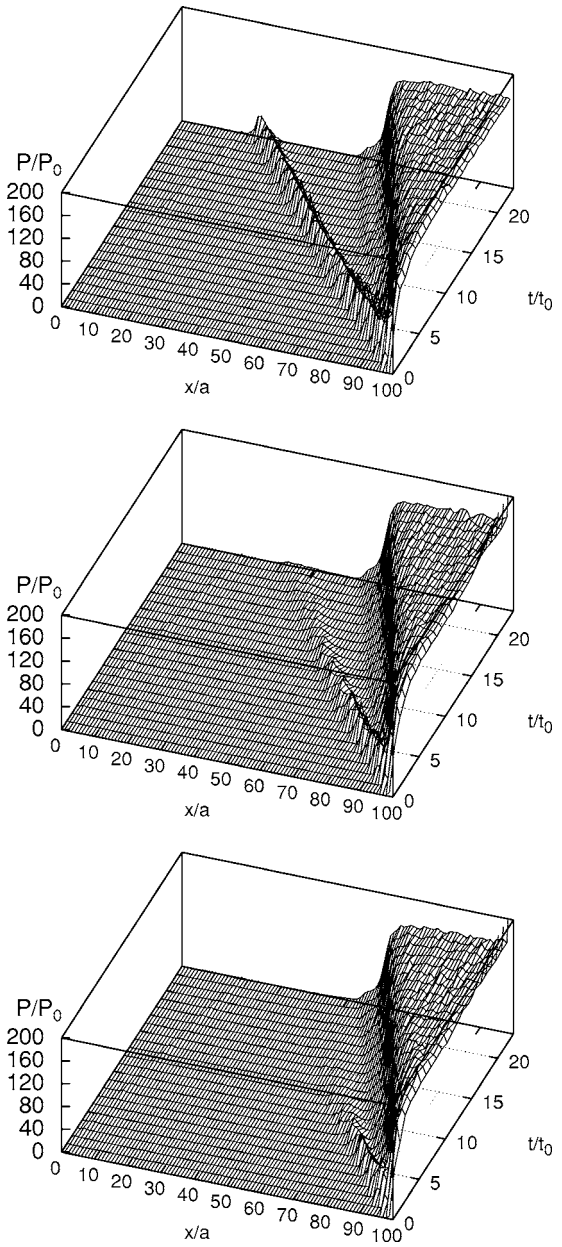

FIG. 4. Damping of the solitary wave at different temperature. From top to bottom: $kT=0.01$, 0.05, and 0.1ϵ. The piston velocity is $u_p/c=0.4$. The solitary waves are visible in front of the transition waves.

2. Temperature dependence

At low temperatures the solitary waves move through the whole sample up to at least $600a$ in the samples with cross section $20\times 20a^2$. At finite temperatures they are damped. The damping increases with temperature: At $u_p/c=0.25$ it becomes visible between $kT/\epsilon=0.03$ and $kT/\epsilon=0.04$ for small samples (see Fig. 4), at $u_p/c=0.4$ the damping starts already between $kT/\epsilon=0.01$ and $kT/\epsilon=0.02$. At higher temperatures solitary waves are no longer present.

B. Properties of the ω-phase

The ω-phase is observed for the first time at the piston velocity $u_p/c=0.05$. Up to $u_p/c=0.1$ the velocity of the interface between bcc and the ω-phase grows much faster than the speed of the following interface with the close-packed phase. If the piston velocity increases further, the transition front speeds up rapidly and at $u_p/c=0.185$ it catches up with the first interface. Now the phase transition goes directly from bcc to the close-packed phase. The ω-phase exists up to temperatures of about $kT/\epsilon=0.15$.

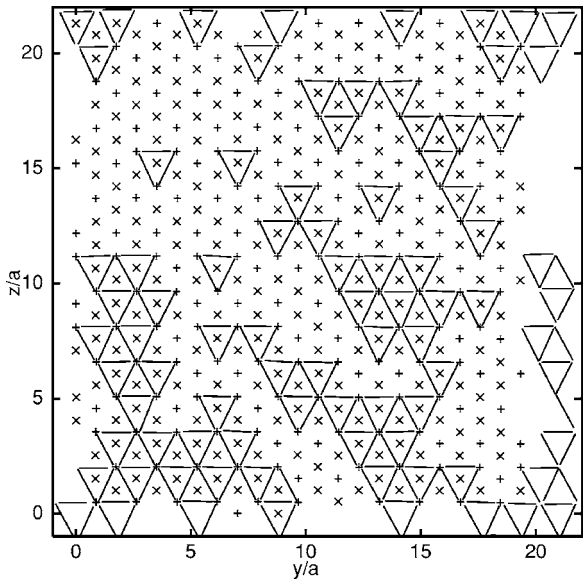

FIG. 5. Cut through the intermediate ω-phase. The crosses indicate one layer, the plus signs the other layer. Both layers together form a triangle lattice. The triangular lattice cells of one variant have been superimposed. The empty triangles are periodic images repeated on the opposite side.

The new phase is created under uniaxial stress. If the stress is released, it slowly transforms back into the bcc phase. Only a few well-separated point defects are left over. This is a further indication of the reversibility of the phase transition.

The bcc phase is a three-layer structure with respect to the $\langle 111\rangle$ direction whereas the new phase possesses only two layers. The whole sample looks triangular in projection (see Fig. 5) since the $\langle 111\rangle$ direction of both phases are aligned. The periodicity perpendicular to the layers is approximately $1a$, and the neighbor cells are either tetrahedra or rectangular pyramids.

The atoms occupy their sites at random in one of the two layers. During simulation they may jump from one layer to the other. There are, however, certain rules for the positioning of the atoms. No clusters of three mutually neighboring atoms (triplets) are permitted. A fractal-looking triangular pattern can be superimposed on the atoms (Fig. 5). Three

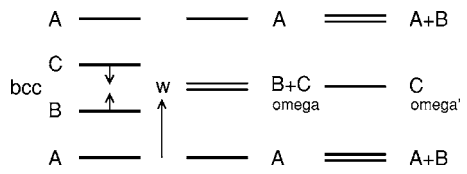

FIG. 6. Transformation from bcc into the ω-phase. Two variants are shown: the collapse of $B+C$ and the collapse of $A+B$.

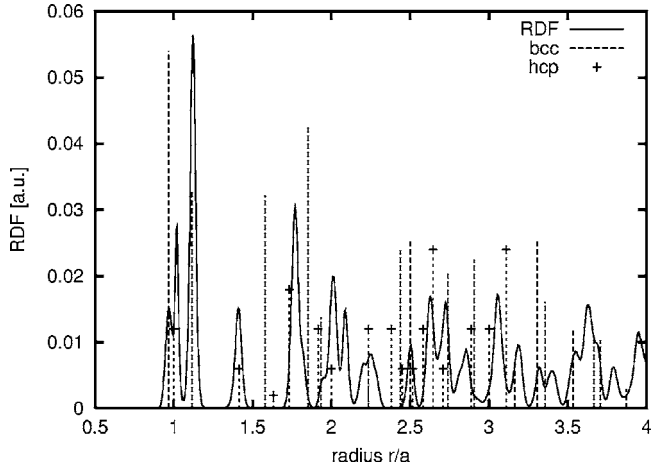

FIG. 7. Radial distribution function of the intermediate phase compared with perfect bcc and hcp. The most prominent disagreement for bcc is visible at around $r=1.4a$. A comparison with uniaxially compressed bcc does not lead to better agreement. The failure of hcp is most prominent at $r=1.75a$. The split first peak clearly indicates that we have no close-packed structure.

so-called variants of the triangular pattern exist which mark different variants. In Fig. 5 only one variant has been drawn for simplicity.

Let us call the three layers of bcc perpendicular to the $\langle 111\rangle$ w axis A, B, and C. The perfect ω-phase is generated if the B and C layers are shifted to the same w coordinate where they form a hexagonal network (Fig. 6). This process is usually called the collapse of the layers.[22] Other variants are created if A and B create layers or the A and B layers collapse.

Both the radial (Fig. 7) and the angular distribution function (Fig. 8) clearly indicate that the ω-phase is a new phase and cannot be mistaken for bcc, the close-packed phases, or any of the other metastable phases studied in paper I.

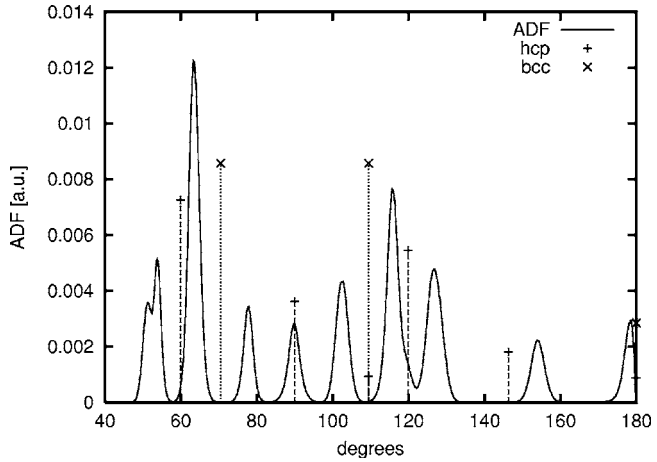

FIG. 8. Angular distribution function of the intermediate phase. The vertical lines indicate the angles in bcc and hcp. The disagreement is obvious. The peak at 147° is lacking in fcc.

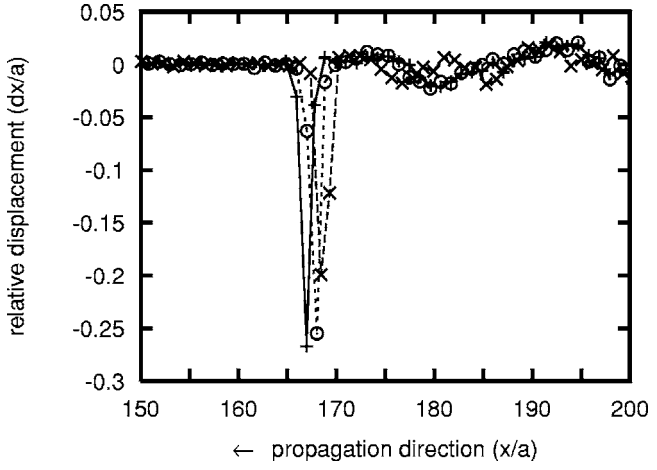

FIG. 9. Displacement of the atoms at the position of a soliton peak. The three signs indicate three arbitrarily chosen chains.

C. Description of the internal structure of the solitary wave peak

The hydrostatic pressure profile shows a maximum with a width of $4-6a$ at the position of the solitary wave (Fig. 2). But if we look at the displacement of the atoms along a certain atom chain we find that the width is $1a$ or at most $2a$. Figure 9 shows the shortening of the distance between the atoms on three arbitrarily chosen chains. At the peak of the solitary wave the distance between two atoms is compressed by 25% to 30%, whereas the preceding and following distances are shortened by 5% to 10%. The other distances are more or less unchanged. The reason for the difference between the width of the hydrostatic pressure and the displacement of the atoms can be seen in the picture: The displacements are not perfectly correlated. After the solitary wave has passed, the atoms are back at their bcc positions. The modulation of the distances behind the solitary wave (Fig. 9) indicate that the longitudinal temperature has risen from $kT=0.001\epsilon$ to about $kT=0.01-0.02\epsilon$.

In Fig. 10 the shocked structure is projected onto a plane perpendicular to the $\langle 111\rangle$ direction. It is apparent that the solitary waves are modulated in the transverse direction and that the transition is reversible.

Figure 11 shows what happens within the solitary wave peak: The three-layer bcc structure is partially transformed into the ω-phase. A perfect transition is impossible since the solitary wave is very thin and fluctuates. The projection of a perfect bcc structure consists of three triangular patterns that are modified within the solitary wave. The circles in Fig. 11 indicate where at this very moment of the simulation the atoms are in the two-layer configuration. Due to the dynamic nature of the solitary wave, these locations are changing permanently.

D. Decay with width

If cross-section averaged histograms of the broad samples (width $40\times 40a^2$ and larger) are plotted (see Fig. 12), it appears as if the solitary waves decay and broaden. But the true reason is not a decrease of the hydrostatic pressure or the

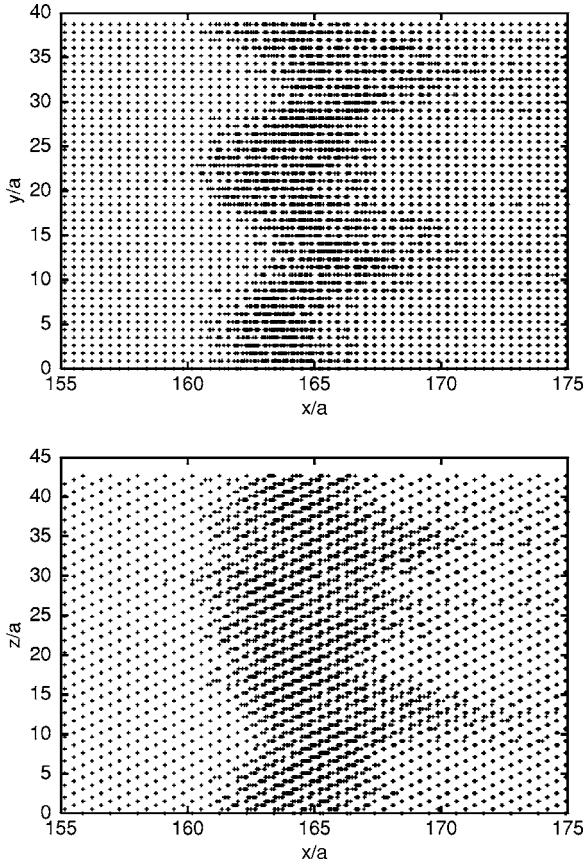

FIG. 10. Projection of the sample with the solitary wave perpendicular to the ⟨111⟩ direction. Upper part: $[2\bar{1}\bar{1}]$ plane, lower part $[01\bar{1}]$ plane. The shock wave moves to the left.

shear strain but a decay of the correlation between the solitary wave peaks on parallel atom chains.

This becomes obvious if we plot the deviation of position of the hydrostatic pressure maxima from the center of mass of the solitary wave (Fig. 13, see also Fig. 10). At the beginning, the manifold formed by the maxima is completely flat. Then it starts to fluctuate randomly. After a while the lowest or second lowest transverse modes, which are compatible with the boundary conditions, start to grow while the higher modes vanish. At the end of the simulation it is no longer possible to represent the maxima by a simply connected manifold.

The decay of the correlation with the width of the sample may render an experimental detection of the solitary waves impossible, especially if the limit of the pressure amplitude of the solitary wave is approaching zero for large widths. Up to now it has not been possible to determine this limit since our computational resources were too limited.

Meanwhile we have repeated wide sample simulations with a softened Dzugutov potential. The decay of the solitary waves is strongly reduced and they are still prominent after a distance of $1000a$. Furthermore, in Kadau *et al.*'s[3] simulations of shock waves in iron, the decay of the solitary waves was much weaker than for the Dzugutov potential. In conclusion, we note that the stability of solitary waves depends strongly on the type of interaction. There is hope for experimental detection since the solitary waves are more stable for realistic interactions.

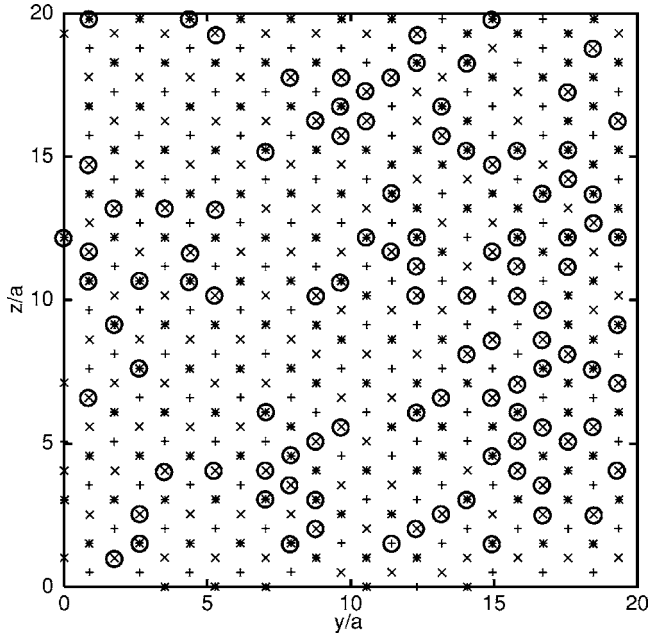

FIG. 11. Cut through the structure at the maximum of a solitary wave peak. The crosses, plus signs, and stars indicate three bcc layers. In a perfect bcc sample, all layers would form a triangular lattice. The black circles indicate the positions where the sequence repeats after two layers, indicating an ω-phase configuration. Compare this figure to Fig. 5.

IV. SHOCK WAVES AND SOLITARY WAVES ALONG ARBITRARY DIRECTIONS

In addition to the main symmetry directions we have looked for solitary waves along a large number of other directions. The amplitude of the hydrostatic pressure at the solitary wave peak at a fixed time $t=4t_0$ has been chosen as a measure of the strength of the solitary waves. This may be a rather crude criterion, but it permits us to get a gross overview.

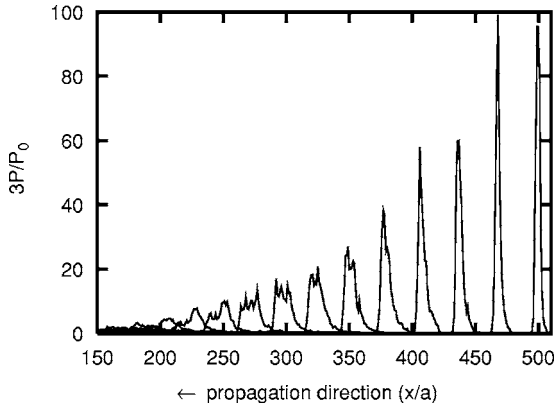

FIG. 12. Decay and broadening of a soliton peak as a function of pressure. The peaks are plotted at equal time intervals.

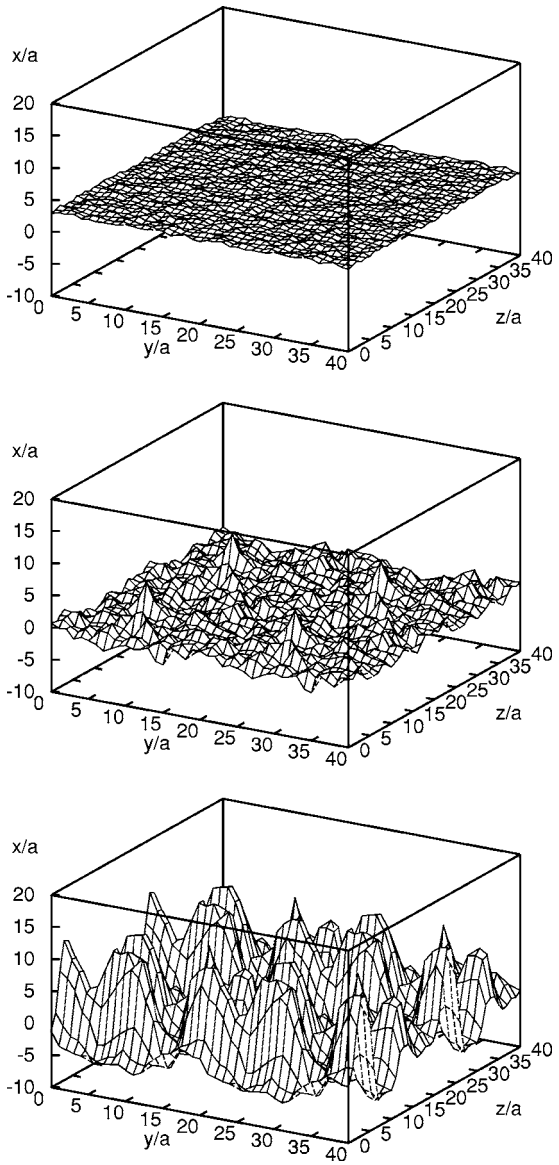

FIG. 13. Deviation of the position of the pressure maxima from the center of mass of the solitary wave. Top: $t=0t_0$, flat one-dimensional wave. Center: $t=2.5t_0$, fluctuations develop. Bottom: $t=7.0t_0$, transverse modulation is present. The piston velocity is $u_p/c=0.4$.

The behavior of solitary waves along arbitrary directions depends strongly on the boundary conditions, i.e., if the momentum mirror method or the collision method is used. In the second case it also depends on the structure of the interface between the two colliding blocks, i.e., if the two blocks form a single crystal or a twin. In all cases, strong solitary waves exist along the threefold axis, whereas no solitary waves are observed around the fourfold and twofold axes and in the directions between them, i.e., in the planes perpendicular to the fourfold axis (see Fig. 14).

In the momentum mirror method the intensity of the solitary waves varies rapidly and unsystematically with direction. The collision of blocks forming a single crystal leads to a continuously decreasing intensity of the solitary waves if the angle to the ⟨111⟩ direction increases (Fig. 14). In the twin case strong solitary waves only exist close to the ⟨111⟩ direction. Along all other directions they are rather weak.

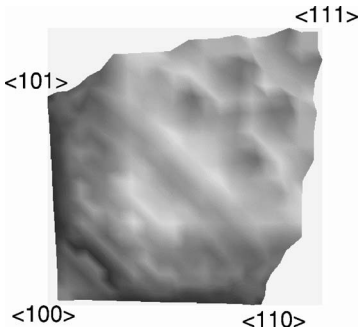

FIG. 14. Strength of the solitary waves as a function of propagation direction for the collision method. Low levels indicate no solitary waves (between ⟨100⟩ and ⟨110⟩, for example). High levels mark strong solitary waves. The increase in soliton strength is best seen between ⟨101⟩ and ⟨111⟩. Unfortunately, the sharp peak along the ⟨111⟩ directions cannot be resolved in the picture.

The reason for the different behavior is rather obvious: In the momentum mirror method we have a rigid boundary; therefore, it should play a role in how the densely packed lattice planes are oriented with respect to it. Extinction effects and a strong angle dependence are expected. In the case of two colliding blocks we have a soft interface. The dense lattice planes will bend and accommodate, which may enhance dissipation. Therefore, a smooth variation of the solitary wave intensity with direction is more likely.

In Fig. 15 we have plotted the atoms in the solitary wave peak for shock waves along the ⟨211⟩ direction simulated by the mirror method. Although the deformation points along the ⟨211⟩ direction, the atoms are shifted along the ⟨111⟩-direction. This is not an exception: If we determine the eigenvectors of the full pressure tensor we find that the strongest compression does not occur parallel to the shock wave direction, but parallel to the ⟨111⟩ direction, except for the mirror planes.

Consequently, there exists only one solitary wave mode for all shock wave directions, namely the one with displacements parallel to the ⟨111⟩ direction. If the material is shocked along an arbitrary direction the solitary wave is excited with lower efficiency. If the shock wave moves in a mirror plane or along a twofold or fourfold axis, no solitary wave can exist, because then two or four ⟨111⟩ directions are equivalent and the superpositions of the displacements cancel.

V. RAMPING LOADING

Two further questions will be addressed now: Are the solitary wave trains merely artifacts of the boundary conditions? Is it possible to suppress them? To avoid the singularity we have changed the simulation setup. In this section, we ramp up the piston velocity linearly from zero to the desired end velocity.

We have tested two cases: $u_{p,end}=5.0v_0$, which is close to the underdriven regime, and $u_{p,end}=8.0v_0$. The results are similar. If the piston acceleration $\dot{u}_p$ is higher than $10v_0/t_0$ in

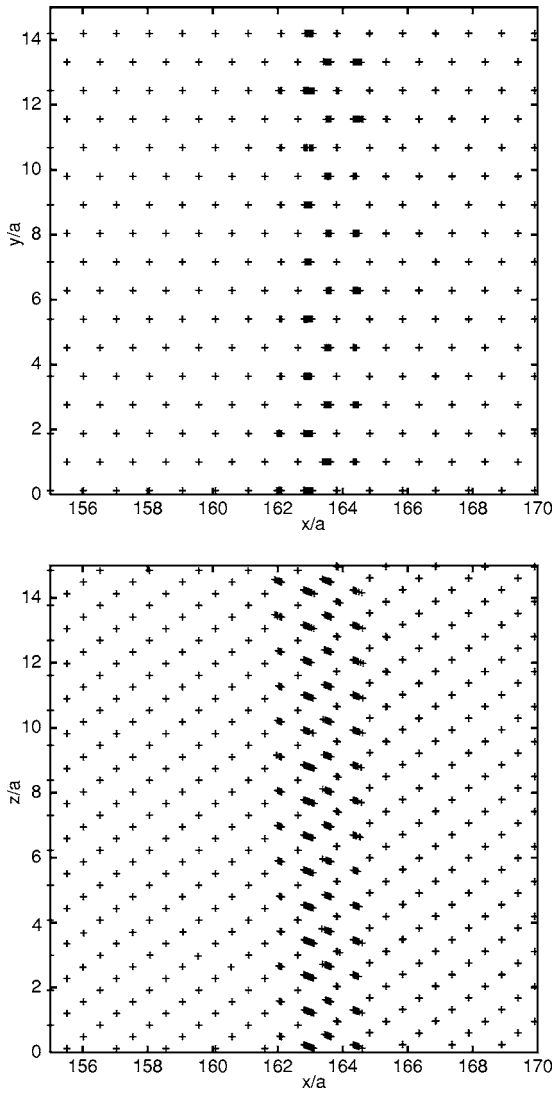

FIG. 15. Solitary wave along the $\langle 211 \rangle$ direction. Upper part: x-y plane, lower part: x-z plane. The wave is currently located between $x=162.5a$ and $x=165a$. Since the y direction is $\langle 01\bar{1} \rangle$ and the z direction $\langle \bar{1}11 \rangle$, we can read of the elongated traces in the center of the lower picture that the displacement of the atoms is not parallel to the deformation along the x direction, but along the $\langle 111 \rangle$ direction.

the case of $u_{p,end}=5.0v_0$ or higher than about $26v_0/t_0$ in the case of $u_{p,end}=8.0v_0$ the velocities of the solitary waves and the velocities of the transformation wave are unchanged. But if the piston acceleration $\dot{u}_p$ is lower than $6.4v_0/t_0$ in the both cases, the solitary waves are eliminated completely. Again, the velocity of the transformation wave remains unaltered. If $u_{p,end}=8.0v_0$ the situation is a little more complicated: up to $\dot{u}_p \approx 14.5v_0/t_0$ a rapid deceleration of the solitary wave is observed but above this threshold the slowing down is reduced and a second solitary wave shows up.

In the transition range between the unaffected behavior and the eliminated solitary waves, the system behaves as if it would be shocked with a piston velocity $u_{p,eff} < u_{p,end}$. This means that we observe the whole sequence of pressure profiles that have been presented as a function of u_p in Sec. III A. But we have to keep in mind that the slowdown happens only virtually since now the phase transition velocity is constant, no matter how large $\dot{u}_p$ is.

The results demonstrate that the solitary waves are an inherent feature of the system and not an artifact of the boundary conditions. They may be delayed and slowed down, but they are still present. On the other hand it may appear as if the solitary waves are rather fragile since they can be suppressed by a slow enough acceleration of the piston, but the question is if this is an appropriate description of the experiment.

Similar results have been obtained if the symmetric impact method is used. Then the singularity is softened, but the solitary waves remain unchanged.

VI. ORIGIN AND STABILITY OF THE ω-PHASE

There are two reasons why the ω-phase forms under uniaxial compression: viewed in reciprocal space bcc possesses a soft mode that leads to the layer collapse and explains the phase modulation; when regarded in physical space bcc becomes energetically unstable with respect to the ω-phase under uniaxial compression. In the following sections we will present these results in more detail.

A. Characterizations of the ω-phase transition

There are two dynamical descriptions of the transition from bcc to the ω-phase that are appropriate for the interpretation of our simulation results. One picture works in reciprocal space and the other in physical space.

1. Longitudinal displacement wave picture

The ω-phase can be generated by a longitudinal phonon wave with wave vector $\mathbf{k}=\frac{2}{3}[111]2\pi/a$ and amplitude $\sqrt{3}/12a$.[24,25] If the wave vector is different from the ideal value, a modulated structure is created with an incomplete collapse or stacking faults. A wrong amplitude can have the same effect as a wrong wave vector. A further variation is the lock-in to a sequence of bcc and ω variants,[26] which is found in our simulations for piston velocities in the range between $u_p/c=0.2$ and 0.3.

2. Atomic row movement picture

In contrast to fcc it is not very appropriate to describe bcc as a stacking of layers, but as a hexagonal arrangement of close-packed atom chains. The basic defects are relative displacements of the chains and not stacking faults since the atoms along a chain move in correlation but neighboring chains interact rather weakly. This view is also very important for the explanation of the solitary waves (see Sec. VII A) and is supported by Monte Carlo simulations by de Fontaine and Buck[27] of the thermal ω-phase transition. Especially their Fig. 9 and the central part of Fig. 10 are similar to our Fig. 5.

A related description has been put forward by Petry *et al.*[28] in the explanation of the behavior of β-Ti (which transforms into an ω-phase). They even call the behavior of the

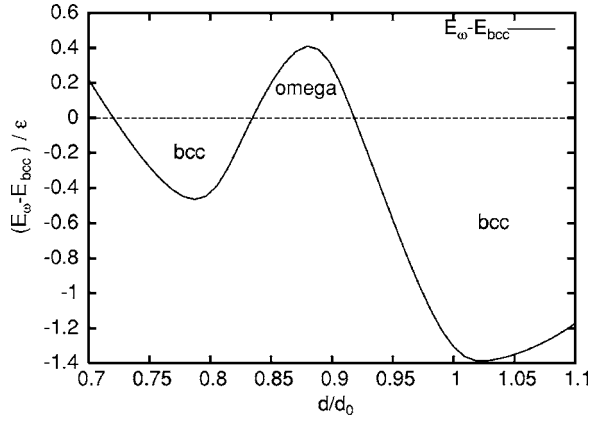

FIG. 16. Difference between the potential energies of bcc and the ω-phase with respect to uniaxial compression. d_0 denotes the equilibrium lattice constant along the [111] or z direction.

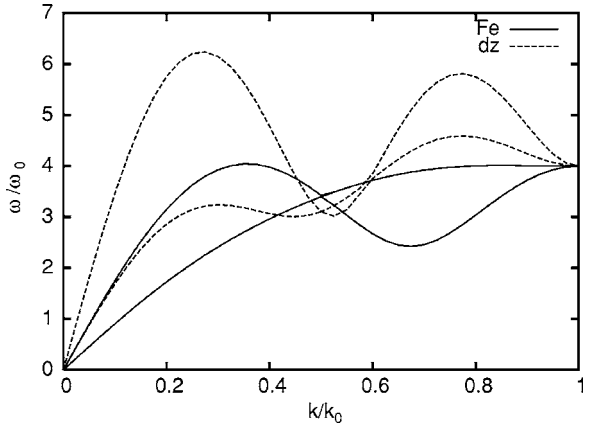

FIG. 17. Phonon dispersion along the [111] direction for iron and for the Dzugutov potential. The upper branches near $k=0$ are the longitudinal waves, the lower branches the transverse modes. The phonon dispersion relations for other bcc metals look similar to iron. They all possess a minimum around $k/k_0=2/3$. The scaling has been chosen such that $\omega=\omega_0$ at $k=k_0$.

atom chains in β-Ti "liquid-like," which means that the transverse motion is localized and the correlation is lost rapidly.

The atomic row picture fits best for weak shock waves below $u_p/c=0.175$: we find a distribution of the atoms in the ratio 0.444:0.556 (±0.002) into the two ω-phase layers and not a ratio of 1:2, which would be expected for the perfect ω-phase. The reason is the following: There are three variants of the ω-phase depending on how the layers collapse ($A+B$, $B+C$, or $C+A$). Since the variants have to fit together coherently, there has to be an adjustment between the variants that changes the expected distribution of the atoms in the three-layer structure from 1:2 to 4:5.

B. Stability of the ω-phase in Dzugutov materials

At first sight there seems to be no reason why the ω-phase should form in Dzugutov materials. The potential energy at the optimum differs by about 1.4ϵ between bcc and the ω-phase, and the ω-phase is never stable with respect to bcc, the σ-phase, and close-packed phases if only isotropic deformations are permitted.

This picture changes completely if the bcc phase is compressed uniaxially as it happens in the shock wave simulations: at a compression of $d/d_0=0.917$ ($d_0=\sqrt{3}/2a$ is the axial lattice constant of bcc in hexagonal representation) the ω-phase becomes more stable than bcc, but at $d/d_0=0.835$ the stability switches back to bcc (see Fig. 16). Remarkably, bcc and the ω-phase both have their optimal lattice constant in the ⟨111⟩ plane at the same value $b=1.76a$ ($b=\sqrt{2}a$ is the planar lattice constant of bcc in hexagonal description), which means that there is no lattice mismatch and no transversal stress is created by the shock wave and the phase transformation. Furthermore, there is no barrier between bcc and the ω-phase if the potential energy is considered as a function of the lattice parameters b and d and the position w/d of the collapsing layers. The optimal aspect ratio b/d is also similar for bcc ($b/d=0.614$) and the ω-phase ($b/d=0.574$).[40]

The stability of the bcc and the ω-phase switches several times with increasing compression (see Fig. 16), but this is irrelevant since the absolute potential energy increases rapidly. It reaches 1.2ϵ at a compression of $d/d_0=0.835$, and 88ϵ at the next intersection at $d/d_0=0.71$. Bcc is no longer stable at this compression.

The instability of bcc at a compression of $d/d_0=0.917$ is the reason for the transition to the ω-phase. The reentrance of the bcc phase stability at $d/d_0=0.835$ causes the modulation of the phase and the solitary wave phenomenon.

C. Phonon dispersion and softening

We have applied the Born–von Kármán theory (for an overview see Born and Huang[29]) to compute the phonon dispersion relation for bcc with the Dzugutov potential in the harmonic approximation and to see if there is indeed a soft mode that would support the longitudinal displacement wave picture.

We find that a soft mode (minimum in the dispersion relation) occurs at $\mathbf{k}=0.52[111]2\pi/a$ already and not at the ideal value $\mathbf{k}=\frac{2}{3}[111]2\pi/a$ (Fig. 17).

The strong offset leads to a modulation of the structure with a frequency of $d_{\mathrm{mod}}=4a$. This value agrees well with the shortest modulation observed in the simulations. If the bcc structure is compressed, the soft mode shifts toward the ideal value, which means that the modulation length rises rapidly, in agreement with the simulations (Fig. 18).

D. Landau-Ginsburg description of the ω-phase transition

Cook[30–33] has worked out a one-dimensional Landau theory to explain the transition between the ω-phase and bcc. The order parameter η is equated to the amplitude of the $\frac{2}{3}[111]2\pi/a$ phonon. A modulated phase occurs if the minimum of the free energy in reciprocal space shifts with changing Landau parameters. Sanati and Saxena[34,35] have extended the theory by including a spatial gradient (Ginsburg) term. This leads to kinks describing phase boundaries between the

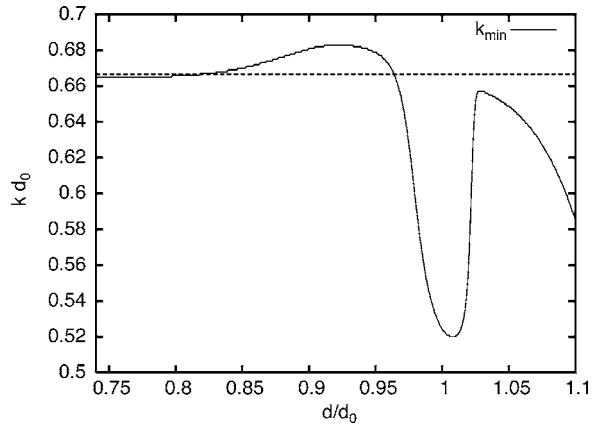

FIG. 18. Position of the minimum of the longitudinal [111] phonon as a function of compression. The line at $kd_0=2/3$ indicates the ideal wave length.

ω-phase and bcc, to the presence of solitons as kink-antikink pairs, and to the existence of soliton lattices.

The Landau free energy F at $T=0$ is equivalent to the potential energy E_{pot}. Since we know the potential energy surface of the partially collapsed ω-phase for the Dzugutov potential as a function of the compression d/d_0 and the shift of the layers w/d, we can easily compute the parameters of the Landau free energy

$$F = F_0 + H\eta + \frac{A}{2}\eta^2 + \frac{B}{3}\eta^3 + \frac{C}{4}\eta^4.$$

The familiar temperature dependence T/T_0-1 is replaced by a compression dependence d/d_0. The relation between the order parameter η and the layer shift w/d has been given by Dmitriev *et al.*[36]

$$\eta = \frac{2}{3}\left[\sin\left(2\pi\frac{w}{d}+\frac{\pi}{6}\right)-\frac{1}{2}\right].$$

We find that the linear coefficient H is almost zero, which indicates that bcc is always close to an extremum. But in contrast to the ordinary behavior of a Landau description where A should be a function of d/d_0 and B and C should be constant, we observe that all parameters are strongly dependent on d/d_0. The situation is even worse: B and C are directly proportional and vary much stronger as a function of d/d_0 than the parameter A. They even change signs in the range of interest.

A second Landau condition is also violated: the coexistence of stable and metastable phases that switch their roles. Two phases coexist only in the ranges between $d/d_0=0.77$ and 0.78 and between 0.82 and 0.92. The second range is interesting since it explains the presence of the ω-bcc phase modulations. The ω-phase is not metastable but represents a local maximum for other compressions d/d_0.

In conclusion we find that the transformation from bcc to the ω-phase can be explained in the spirit of a Landau theory but a quantitative application fails since the prerequisites for the Landau theory are not fulfilled.

VII. THEORETICAL EXPLANATIONS OF THE SOLITARY WAVES

We will present a crude model in which we claim that the solitary waves occur along the direction where the atoms have the shortest distance and that the solitary waves are quasihard sphere collisions in the spirit of Nesterenko.[38] This model is also similar to the beads-on-a-wire model. We have tested the model for different lattices and proved that it works for all cases where solitary waves have been observed up to now.

A. Crude model for the solitary waves

The solitary waves can be understood in a crude model that assumes that the origin is direct hits of close-neighbor quasihard spheres. The directions in bcc where the atoms form chains with distances of the potential radius $1a$ are exactly the $\langle 111\rangle$ directions. These chains are close-packed. In a characteristic soliton peak the distance between two atoms is reduced by 25%. The potential energy increases to about 21ϵ, which is large, and the interaction can be regarded as a hard collision. (If the compression is 30%, the energy grows to 70ϵ.) If shocked along a fourfold or twofold direction, the momentum of the moving atom points directly into a gap between two atoms, and no direct collision partner is present. The increase in energy at the same displacement is only 4.3ϵ for the fourfold direction and for the twofold direction it is negligible. Therefore solitary waves cannot persist.

In the transverse direction a loss of correlation leads to a small increase of the binding energy only. Thus the decay of the solitary waves by transverse fluctuations is reasonable.

In the metastable phases of the Dzugutov potential, the σ phase, and the quasicrystal, transient solitary waves are observed if the samples are shocked perpendicular to the basic square-triangle layer direction (for details see paper I). No solitary waves are observed if shock wave direction is inclined at an angle of 45° or 90° with respect to the basic layers. The reason is that the close-packed chains of atoms are thinned out in these phases by other atom arrangements. Therefore the solitary waves are not stable if the materials are shocked perpendicular to the basic layers. In the plane of the basic tiles, in the quasicrystalline plane, and in the 45° directions there are no well-defined atomic chains at all, thus no solitary waves can exist.

May this model work for other structures as well? In fcc the solitary waves are found along the twofold directions, which are the close-packed chains. The model also works for a specially prepared simple cubic crystal where the solitary waves can be switched on and off along the fourfold direction if the interaction is tuned such that it is strong along the fourfold or twofold direction.

B. Tunable solitary waves

To figure out how reasonable our model is we have tried to generate solitary waves in simple cubic (sc) crystals. Since the coordination number of sc crystals is only six, they are not stable with respect to shear distortion if isotropic poten-

tials are used. We have therefore introduced two sets of bonds: Nearest neighbors along the fourfold direction interact with one set, and the next-nearest neighbors along the twofold direction interact with the other set. We can tune the relative strength r_s of these two sets of interactions. If the next-nearest-neighbor interactions are strong then the system behaves as if it would consist of two independent interpenetrating fcc crystals. The depth of the edge-connected atoms has been kept fixed at $v_e=-1\epsilon$, the strength for diagonal-connected atoms has been varied between $v_d=-0.25$ and -4ϵ.

The results follow. Along the fourfold direction solitary waves are observed for any value of r_s as predicted by our crude model, since these atoms always have the shortest distance. If the shock wave propagation is along twofold direction, we find solitary waves only for large r_s as known from the fcc crystals[2] since in the case of large r_s second-nearest neighbors have direct contact. The crossover occurs between $r_s=v_d/v_e=0.5$ and 1.0. Shock waves along the $\langle 111\rangle$ direction never lead to solitary waves even in the case of extremely high piston velocities. These results nicely fit into the predictions of our crude model.

C. Continuum approach

The simplest description of solitary waves in one-dimensional crystals involves Korteweg–de Vries (KdV) and Toda solitons.[17] Thus a natural extension would be the Kadomtsev-Petviashvili (KP) solitary waves,[37] which are nonlinear along one direction and linear in the transverse directions. Moreover, these solitary waves include the KdV and Toda solitons as one-dimensional limits. There exist two varieties, one with positive and the other with negative dispersion for the transverse part. The solitons of KPI equation behave indeed like our solitary waves, i.e., they decay into so-called bullets similar to what we have seen in Fig. 13. An application of this approach is currently far beyond the scope of this paper since up to now not even the general continuum case has been treated (which has to be solved numerically) and in our case the discrete limit would be needed.

VIII. DISCUSSION

Holian *et al.*[16] have simulated shock waves in one-dimensional lattice models and described the results by analytical means.[17] For Toda interactions they could show that solitary wave trains exist. Morse and Lennard-Jones potentials can be treated as perturbations of the Toda interaction. The important parameter is the product $\alpha\nu$ of the relative anharmonicity $\alpha=-a_0\Phi'''(a_0)/\Phi''(a_0)/2$ of the potential $\Phi(r)$ at its minimum a_0 and the relative piston velocity $\nu=u_p/c$ with respect to the velocity of sound c. The entire shock profile may be described as a soliton wave train. If $\alpha\nu$ is small, the continuum KdV description can be applied and the discrete Toda description if it grows. Isolated solitons exist near the shock front. At small u_p they separate logarithmically; at large u_p they are locked in a periodic pattern. If one moves from the shock front to the piston, the phase between neighboring particles increases until it reaches π. Near the piston the particles are in an optical mode, their displacement is equal and opposite. The optical mode is the highest wave number that a discrete lattice can support. If $\alpha\nu$ is small, the long time behavior is quasiharmonic, and hard-rod-like otherwise. The crucial point is that the system is one dimensional, which prevents plasticity since the particles cannot change their order. No dissipation is present. In three dimensions we have dissipation due to the possibility of transverse motion. A comparison of the predicted speed of the leading soliton $u_s/c=1+2/3\alpha\nu$ for small amplitudes (weak shock waves) and $u_s/c=2\alpha\nu/\ln(4\alpha\nu)$ for large amplitudes (stronger shock waves) with the propagation speed of our solitary waves shows that there is no agreement.

The one-dimensional results also hold in three dimensions, if the shock strength is below the Hugoniot elastic limit, in the elastic-plastic regime, or if the temperature is zero.[9,16] Then there are steady solitary waves locked-in to an oscillatory profile. Holian[9] claims that if the cross section of the samples is too small, distortions will be locked out and lead to an ever-growing nonsteady soliton profile. He is referring to Germann *et al.*'s[2] simulations in the elastic-plastic regime with cross sections of up to $200\times 200a^2$. We have observed nonsteady solitary waves in the overdriven regime in samples with up to $120\times 120a^2$. But we found that the averaged solitary waves are decaying by losing the interchain correlation, while the solitary waves on a single atom chain persisted.

Results similar to ours have been found by Kadau.[3] He studied bcc iron equipped with different sets of EAM potentials. In general his results are very similar to ours, at least for the $\langle 111\rangle$ direction. The solitary wave trains in his simulations seem to consist of more peaks than in our cases and to decay more slowly. A direct comparison, however, is lacking. There are, however, some notable differences.

(1) No ω-phase has been observed. The reason is unclear. Since we have shown that the ω-phase and the solitary waves are two sides of the same phenomenon, and solitary waves have been observed in both cases, one should expect the ω-phase in both systems.

(2) A modulated ω-phase may not be present in iron since the softening would occur close to the ideal wave vector.

(3) The solitary waves in Kadau *et al.*'s simulations are not modulated in the transverse direction although the cross sections are large enough. Since they do not lose their correlation they decay much slower. Meanwhile we could demonstrate that our solitary waves become much more stable if we soften the potential somewhat, but the transverse modulations can still be detected, although they are much weaker. Further reasons might be the many-body part of the EAM interaction or the low stability of bcc with the Dzugutov potential.

ACKNOWLEDGMENTS

Part of this research has been carried out at the Los Alamos National Laboratory. Financial support from LANL and SFB 382 is greatly acknowledged. The author also thanks Kai Kadau and Professor Dr. H.-R. Trebin for many helpful discussions.

[1] J. Roth, preceding paper, Phys. Rev. B **72**, 014125 (2005).
[2] T. C. Germann, B. L. Holian, P. S. Lomdahl, and R. Ravelo, Phys. Rev. Lett. **84**, 5351 (2000).
[3] K. Kadau, T. C. Germann, P. S. Lomdahl, B. L. Holian, and F. J. Cherne, in *Shock Compression of Condensed Matter—2003*, edited by Michael D. Furnish, and Jerry W. Forbes, and Yogendra M. Gupta, AIP Conf. Proc. No. 706 (AIP, New York, 2004), p. 229.
[4] S. Zybin, V. V. Zhakhovskiĭ, M. L. Elert, and C. T. White, *Shock Compression of Condensed Matter—2003*, Ref. 3, p. 310.
[5] B. L. Holian, Phys. Rev. A **37**, 2562 (1988).
[6] J. P. Hirth, R. G. Hoagland, B. L. Holian, and T. C. Germann, Acta Mater. **47**, 2409 (1999).
[7] D. Tanguy, M. Mareschal, P. S. Lomdahl, T. C. Germann, B. L. Holian, and R. Ravelo, Phys. Rev. B **68**, 144111 (2003).
[8] T. C. Germann, D. Tanguy, B. L. Holian, P. S. Lomdahl, M. Mareschall, and R. Ravelo, in Minerals, Metals & Mater. Soc. and ASM Int. Metallurgical & Mater. Trans. A-Physical Metallurgy & Mater. Sci., Vol. 35A, (9), pp. 2609–2615.
[9] B. L. Holian, in *High-Pressure Shock Compression of Solids VI*, edited by Y. Horie, L. Davison, and N. N. Thadhani (Springer, New York, 2002), p. 149.
[10] E. M. Bringa, B. D. Wirth, M. J. Caturla, J. Stölken, and D. Kalantar, Nucl. Instrum. Methods Phys. Res. B **202**, 56 (2003).
[11] S. V. Zybin, M. L. Elert, and C. T. White, Phys. Rev. B **66**, 220102(R) (2002).
[12] V. V. Zhakhovskiĭ and S. V. Zybin, Seminário Brasileiro de Análise (1999), Vol. 49, p. 635.
[13] V. V. Zhakhovskiĭ, S. V. Zybin, K. Nishihara, and S. I. Anisimov, *Proceedings of the Japanese Symposium on Shock Waves, Aoyama Gakuin University, Tokyo, Japan, March 19-21, 1999*, p. 241.
[14] V. V. Zhakhovskiĭ, S. V. Zybin, K. Nishihara, and S. I. Anisimov, Phys. Rev. Lett. **83**, 1175 (1999).
[15] V. V. Zhakhovskiĭ, S. V. Zybin, K. Nishihara, and S. I. Anisimov, Prog. Theor. Phys. Suppl. **138**, 223 (2000).
[16] B. L. Holian and G. K. Straub, Phys. Rev. B **18**, 1593 (1978); G. K. Straub, B. L. Holian, and R. G. Petschek, Phys. Rev. B **19**, 4049 (1979).
[17] B. L. Holian, H. Flaschka, and D. W. McLaughlin, Phys. Rev. A **24**, 2595 (1981).
[18] T. C. Germann, B. L. Holian, and P. S. Lomdahl, Proc. of the 9th American Physical Society Topical Conference on Shock Compression of Condensed Matter, edited by M. D. Furnish, L. C. Chhabildas, and R. S. Hixson, AIP Conf. Proc. No. 505 (AIP, NY, 2000), p. 297.
[19] B. L. Holian and P. S. Lomdahl, Science **280**, 2085 (1998).
[20] K. Kadau, Ph.D. thesis, Universität Duisburg, 2001.
[21] C. M. Wayman and H. K. D. H. Bhadeshia, in *Physical Metallurgy*, edited by R. W. Cahn and P. Haasen (North Holland, Amsterdam, 1996), Vol. II, p. 1546.
[22] S. Sikka, Y. K. Vohra, and R. Chidambaram, Prog. Mater. Sci. **27**, 245 (1982).
[23] L. M. Hsiung and D. H. Lassila, Acta Mater. **48**, 4851 (2000).
[24] D. de Fontaine and R. Kikuchi, Acta Metall. **22**, 1139 (1974).
[25] D. de Fontaine, Mater. Trans. A **19**, 169 (1988); **29**, 585 (1973); **29**, 594 (1973); B. Horovitz, J. L. Murray, and J. A. Krumhansl, Phys. Rev. B **18**, 3549 (1978).
[26] J. M. Sanchez and D. de Fontaine, J. Appl. Crystallogr. **10**, 220 (1977).
[27] D. de Fontaine and O. Buck, Philos. Mag. **71**, 967 (1973).
[28] W. Petry, A. Heiming, J. Trampenau, M. Alba, C. Herzig, H. R. Schober, and G. Vogl, Phys. Rev. B **43**, 10933 (1991).
[29] M. Born and K. Huang, *Dynamical Theory of Crystal Lattices* (Clarendon Press, Oxford, 1954).
[30] H. E. Cook, Acta Metall. **21**, 1445 (1973).
[31] H. E. Cook, Acta Metall. **22**, 239 (1974).
[32] H. E. Cook, Acta Metall. **22**, 1027 (1975).
[33] H. E. Cook, Acta Metall. **22**, 1041 (1975).
[34] M. Sanati and A. Saxena, Physica D **123**, 368 (1998).
[35] M. Sanati and A. Saxena, Am. J. Phys. **71**, 1005 (2003).
[36] V. P. Dmitriev, S. B. Rochal, Y. M. Gufan, and P. Toledano, Phys. Rev. Lett. **60**, 1958 (1988).
[37] E. Infeld and G. Rowlands, *Nonlinear Waves, Solitons, and Chaos* (Cambridge University Press, Cambridge, 2000).
[38] V. Nesterenko, in *Dynamics of Heterogeneous Materials* (Springer, New York, 2001), Chap. 2, p. 1.
[39] Reduced units are used throughout the paper. Lengths are given in a and energies in ϵ. All other values are expressed by these two and the mass m. Thus we have $t_0=a\sqrt{m/\epsilon}$, $v_0=\sqrt{\epsilon/m}$, and $P_0=\epsilon/a^3$
[40] On the other hand, there is no low-lying transition path from bcc to the high-pressure fcc phase, which also lies in the given parameter space, since bcc and fcc both have $w/d=1/3$, but different aspect ratios $b/d=2.457$